



**HAL**  
open science

## Understanding XANES spectra of two-temperature warm dense copper using ab initio simulations

N. Jourdain, V. Recoules, L. Lecherbourg, P. Renaudin, F. Dorchie

► **To cite this version:**

N. Jourdain, V. Recoules, L. Lecherbourg, P. Renaudin, F. Dorchie. Understanding XANES spectra of two-temperature warm dense copper using ab initio simulations. *Physical Review B*, 2020, 101 (12), 10.1103/PhysRevB.101.125127 . hal-03009008

**HAL Id: hal-03009008**

**<https://hal.science/hal-03009008>**

Submitted on 17 Nov 2020

**HAL** is a multi-disciplinary open access archive for the deposit and dissemination of scientific research documents, whether they are published or not. The documents may come from teaching and research institutions in France or abroad, or from public or private research centers.

L'archive ouverte pluridisciplinaire **HAL**, est destinée au dépôt et à la diffusion de documents scientifiques de niveau recherche, publiés ou non, émanant des établissements d'enseignement et de recherche français ou étrangers, des laboratoires publics ou privés.

**Understanding XANES spectra of two-temperature warm dense copper using *ab initio* simulations**N. Jourdain,<sup>1,2</sup> V. Recoules<sup>ⓧ,1,\*</sup> L. Lecherbourg,<sup>1,3</sup> P. Renaudin,<sup>1</sup> and F. Dorchies<sup>2</sup><sup>1</sup>CEA-DAM-DIF, F-91297 Arpajon, France<sup>2</sup>Université Bordeaux, CNRS, CEA, CELIA, UMR 5107, F-33400 Talence, France<sup>3</sup>LOA, ENSTA ParisTech, CNRS, Ecole Polytechnique, Université Paris-Saclay, F-91120 Palaiseau, France

(Received 18 March 2019; revised manuscript received 13 February 2020; accepted 27 February 2020; published 26 March 2020)

Using *ab initio* molecular-dynamics simulations combined with linear-response theory, we studied the x-ray absorption near-edge spectra (XANES) of a two-temperature dense copper plasma. As the temperature increases, XANES spectra exhibit a pre-edge structure balanced by a reduction of the absorption just behind the edge. By performing systematic simulations for various thermodynamic conditions, we establish a formulation to deduce the electronic temperature  $T_e$  directly from the spectral integral of the pre-edge that can be used for various thermodynamic conditions encountered in a femtosecond heating experiment where thermal nonequilibrium and expanded states have to be considered.

DOI: [10.1103/PhysRevB.101.125127](https://doi.org/10.1103/PhysRevB.101.125127)

Time resolved x-ray absorption near-edge spectroscopy (TR-XANES) was recently extended to the warm dense matter (WDM) regime [1]. This highly transient physics has required specific development to get an appropriate time-resolution (picosecond or less) on XANES measurements. TR-XANES gives a complete picture by probing simultaneously the valence electrons and the atomic local arrangement modifications in WDM situations well beyond the melting. However, the physical interpretation of XANES spectra is not straightforward and a strong connection between theory and experiment is needed to extract information. This issue has been addressed using *ab initio* molecular dynamics (AIMD) simulations, providing a consistent description of both the electronic and ionic structures, together with x-ray absorption spectra calculation [2,3].

In the past decade, both theoretical and experimental XANES spectroscopy was used to get a deep understanding of the electronic structure modification of metals in the WDM. On aluminum, XANES modification during the solid-liquid-vapor phase transition was observed with picosecond time resolution [4]. With the support of AIMD simulations, this has shown the connection between electronic and ionic modifications. Comparison between measurements and calculations for molybdenum have demonstrated that XANES spectra can be simply interpreted in terms of electron DOS modification when solid molybdenum turns to WDM [5]. Besides the understanding of the phenomena involved, it is possible to have access to the time scales of phase transitions [4,6,7]. XANES spectra were also used to shed light on the DOS modification induced by laser shock compression in metals such as aluminum [8,9] and iron [10,11].

When WDM is transiently produced by femtosecond laser heating, matter faces nonequilibrium situations. It is a great

scientific challenge to independently resolve the electron and ion dynamics. In principle, TR-XANES can address this physics, but it is necessary to disentangle the corresponding features in XANES spectra, which depend on the considered element. In some light metals such as Be [12] and Al [13], the electronic temperature can be retrieved directly from the slope of the absorption  $K$  edge. In most metals with a localized  $d$  band, the situation is more complex and this methodology cannot be applied. Recent experiments have been dedicated to femtosecond laser-heated warm dense copper on a synchrotron beamline [3,14]. Using 2-ps time-resolved x-ray spectroscopy, Cho *et al.* investigated the modification of XANES spectra near the  $L_{2,3}$  edge. By direct comparison between measured spectra and spectra computed using AIMD, they retrieved the time evolution of the electron temperature and compare it to the behavior obtained using a two-temperature model.

The purpose of the present paper is to go further in the calculations and analysis of warm dense copper using AIMD simulations. The interpretation of XANES spectra especially for transition metal is nontrivial and requires a careful analysis. The relation between the electronic temperature  $T_e$  and pre-edge peak is reproduced. A quasilinear function is extracted to deduce absolute values of  $T_e$  (up to 3 eV) from the spectral integration of the pre-edge. The impacts of ion temperature  $T_i$  and density are carefully and independently studied. This shows the validity of this function in the various thermodynamic conditions encountered in a femtosecond heating experiment, including strong thermal nonequilibrium. This provides a practical  $T_e$  diagnostic to analyze any XANES experiment without the need of additional AIMD calculations. It has been used in a recently published paper that revisits the electron-ion thermal equilibration dynamics on a tabletop setup, emphasizing the critical role of target expansion [15]. Other features are identified above the L edge, in close relation with the crystalline structure.

\*vanina.recoules@cea.fr

## I. XANES SPECTRUM AT AMBIENT CONDITION

Before analyzing the modification of XANES spectra induced by electron temperature ( $T_e$ ), ion temperature ( $T_i$ ), and density  $\rho$ , we first need a clear understanding of the connection between XANES spectra and the electronic structure of copper at ambient condition. This is also a way to check the validity and the precision of the method we use.

### A. Computational method

To obtain x-ray absorption spectra of warm dense copper, we first need to generate a set of atomic configurations for a given ( $\rho$ ,  $T_i$ ,  $T_e$ ) condition. AIMD simulations are performed using the *ab initio* plane wave density functional theory (DFT) code ABINIT [16–18]. DFT is applied together with local density approximation [19]. For nonequilibrium AIMD simulations the ion and electron temperatures are controlled independently. While the electron temperature is fixed for every time step in the simulation, the ion temperature is controlled in the iso-kinetics ensemble where the velocity is rescaled at every time step to maintain the desired temperature.

We start the simulations with 108 atoms initially arranged in a perfect fcc lattice. The equilibration for a given temperature is then monitored by looking at the pressure. Before reaching a stable ionic structure, the system relaxes for a few hundreds of time steps during which the pressure increases. After equilibration, it fluctuates around a well-defined value. At the end, the initial configuration is propagated up to 2 ps using time steps of 2 fs for the low temperature and 0.5 fs for temperatures above 1 eV. We consider electronic states occupied down to  $10^{-6}$  electrons per states which means around 1600 bands are explicitly computed for the highest temperature considered here. All molecular dynamics calculations were performed at the  $\Gamma$  point to represent the Brillouin zone. The  $\Gamma$  point sampling is expected to be a good approximation for the calculation of the structure and dynamics of copper. We use for this element a PAW data set generated using 11 outer electrons ( $3d^{10}4s^1$ ) and a cutoff radius of 2 bohr that has been benchmarked against physical properties obtained from experiments [20]. The plane wave cutoff is 15 Ha.

We then select equally spaced ionic configurations along the equilibrated part of the trajectory and compute for each of them the corresponding electronic structure with a DFT calculation. These *ab initio* electronic structure calculations are performed on a  $3 \times 3 \times 3$  Monkhorst-Pack  $\mathbf{k}$ -point grid and with 2500 electronic bands in order to obtain eigenstates converged up to 50 eV above the chemical potential. For this part, the PAW data set includes semicore states with 19 outer electrons ( $3s^23p^63d^{10}4s^1$ ) and a cutoff radius of 2 bohr [20]. Two projectors are used for  $s$  and  $p$  channels, and three projectors for the  $d$  channel. The plane wave cutoff is 25 Ha. These electronic structure calculations provide all the required outputs to compute the absorption cross section.

The absorption cross section is calculated in a single electron picture: an electron makes the transition from a core orbital  $\phi_{\text{core}}$  to an excited state  $\psi_{n,\mathbf{k}}$ . The transition energy corresponds to the energy difference between these orbitals. Then, for a given  $\mathbf{k}$  point, the absorption cross section is

expressed as [21]

$$\sigma_{\mathbf{k}}(\omega) = 4\pi^2\omega \sum_n [1 - f(\epsilon_{n,\mathbf{k}})] \times |\langle \psi_{n,\mathbf{k}} | \vec{\nabla} | \phi_{\text{core}} \rangle|^2 \delta(\epsilon_{\text{core}} - \epsilon_n - \hbar\omega). \quad (1)$$

We employ atomic units, with the electron charge  $e$ , Planck's constant  $\hbar$ , the electron mass  $m_e$ , and the fine structure constant  $\alpha$  all set to unity. The  $n$  summation ranges over the discrete bands (orbitals).  $f(\epsilon_{n,\mathbf{k}})$  is the Fermi-Dirac occupation factor corresponding to the energy  $\epsilon_{n,\mathbf{k}}$  of the  $n$ th band and for the  $\mathbf{k}$ -point  $\mathbf{k}$ . The total cross section is obtained by direct summation over all necessary  $\mathbf{k}$  points.

To take into account the natural linewidth of the levels involved in the transition and the resulting spectral broadening of the absorption edges, we use a Lorentzian function to model the delta function of Eq. (1):

$$\delta(\epsilon_{\text{core}} - \epsilon_n - \hbar\omega) = \frac{1}{\pi} \frac{\Gamma_f(\omega)}{\Gamma_f(\omega)^2 + (\epsilon_{\text{core}} - \epsilon_n - \hbar\omega)^2}. \quad (2)$$

This Lorentzian function has an energy-dependent width  $\Gamma_f$  according to the reference [22] which reads

$$\Gamma_f(\omega) = \begin{cases} 0, & \hbar\omega < E_F \\ \Gamma_{\text{hole}} + \gamma(\omega), & \hbar\omega > E_F \end{cases} \quad (3)$$

This reproduces structures at the  $L_2$  edge broader than the ones at the  $L_3$  edge.

In Eq. (3),  $\Gamma_{\text{hole}}$  is the core level spectral width. The  $\gamma$  function is an arctangent-like function that gives a smooth broadening from  $\Gamma_{\text{hole}}$  to a chosen  $\Gamma_{\text{max}}$  value, and is expressed as:

$$\gamma(\omega) = \Gamma_{\text{max}} \left[ \frac{1}{2} + \frac{1}{\pi} \arctan \left( e - \frac{1}{e^2} \right) \right], \quad (4)$$

where  $e = (\omega - E_F)/(E_{\text{ctr}} - E_F)$  and  $E_{\text{ctr}}$  is the inflection point of the arctangent function.

The core states  $|\phi_{\text{core}}\rangle$  are obtained from an all-electron atomic calculation performed during the generation of our PAW data set using ATOMPAW code [23]. For the  $L_{2,3}$  absorption edge which we consider here, we need the  $\phi_{2p}$  orbitals. The radial parts of the  $2p_{1/2}$  and  $2p_{3/2}$  core wave functions are taken identical. The spin-orbit splitting of the  $2p$  states is introduced by shifting the calculated absorption spectrum by the value of the energy separation between the  $L_3$  and the  $L_2$  edges. It can be obtained from a DFT relativistic all-electron calculation and is equal to 20 eV. The two edges have similar structures, but their intensities are related by a factor of 2 (the statistical branching ratio). Figure 1 shows how the  $L_2$  edge is constructed from the  $L_3$  edge for the XANES spectrum at ambient conditions.

During the experimental measurements of the XANES spectra, the system is modified by the probe itself as an inner-shell electron is removed. In many cases [24], it is necessary to include in the simulation cell one atom described by a PAW data set including a hole in the core shell. This is a way to model the electron-hole interaction but it neglects many-body interactions and dynamic core-hole interaction. In the case of copper, the agreement with the experimental spectrum is better without the consideration of the core hole. This was already observed in Ref. [22]. Quoting Mauchamp *et al.* [24],

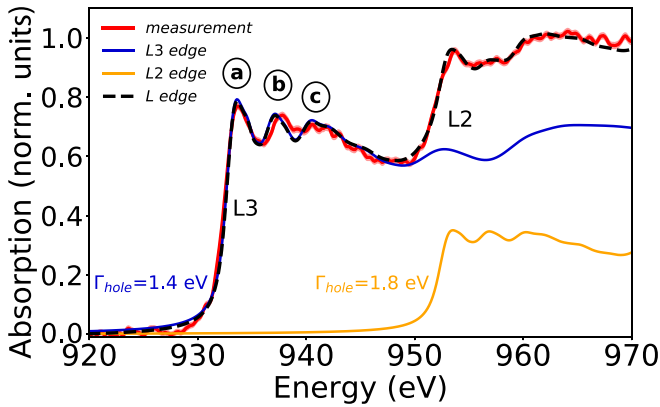


FIG. 1. Constructed XANES spectrum at  $L_{2,3}$  edges (black curve) for the case at ambient conditions ( $\rho_0$ ,  $T_e = T_i = 300$  K), compared to experiment in the same conditions (red curve). The computed  $L_3$  edge (blue curve) and  $L_2$  edge deduced from  $L_3$  (yellow curve) used for the construction are shown.

a core-hole effect is always present in any core-level spectroscopy experiment but its effect is not always evidenced and nothing can be said *a priori* concerning the agreement or not with the experiment. When building the PAW data set with a hole in the core, there is no mean to test those PAW data sets. The only way is to compare directly the XANES spectra with experiment. This was also the choice in Refs. [3,14].

At the end, we compute the absorption cross section for each atom in the simulation box for each snapshot and then do an average on the resulting spectra.

## B. Comparison with experiment

Figure 1 shows the comparison between the theoretical and experimental [15] XANES spectra in ambient conditions. The absolute position of the edge cannot be formally obtained with the present model. To be compared with the experiment, the theoretical spectrum for the cold case is shifted to match the experimental energy position of the edge. The same rigid shift will then be applied to all computed absorption spectra.

The best agreement with the experimental cold spectrum is obtained using  $\Gamma_{\text{hole}} = 1.4$  eV and  $\Gamma_{\text{max}} = 5.1$  eV for the  $L_3$  edge. For the  $L_2$  edge, we use a fixed value of 1.8 eV. These values of  $\Gamma_{\text{hole}}$  are close to the one found in Ref. [25] taken into account the spectral resolution of the experimental spectrum. These values are used for all computed spectra and can be seen in Fig. 1 for both  $L_3$  and  $L_2$  edges.

The agreement between experimental and theoretical spectra is excellent. The first three peaks above the  $L_3$  edge [labeled (a), (b), and (c)] and the minimum around 950 eV are well reproduced. The spectral shape and amplitude of the  $L_2$  edge are also well described by the theoretical spectrum.

$L_{2,3}$  edges probe the unoccupied  $s$  and  $d$  states. This is illustrated in Fig. 2 showing the density of state projected on  $s$  and  $d$  channels together with the corresponding XANES spectrum at the  $L_3$  edge.  $p$  states are not shown here as they do not contribute to the absorption cross section because of the selection rule  $\Delta l = \pm 1$ . For copper at ambient conditions, the  $3d$  states are entirely occupied and the XANES spectrum reflects the  $s$ - and  $d$ -type orbitals above the chemical potential  $\mu(T_e)$ .

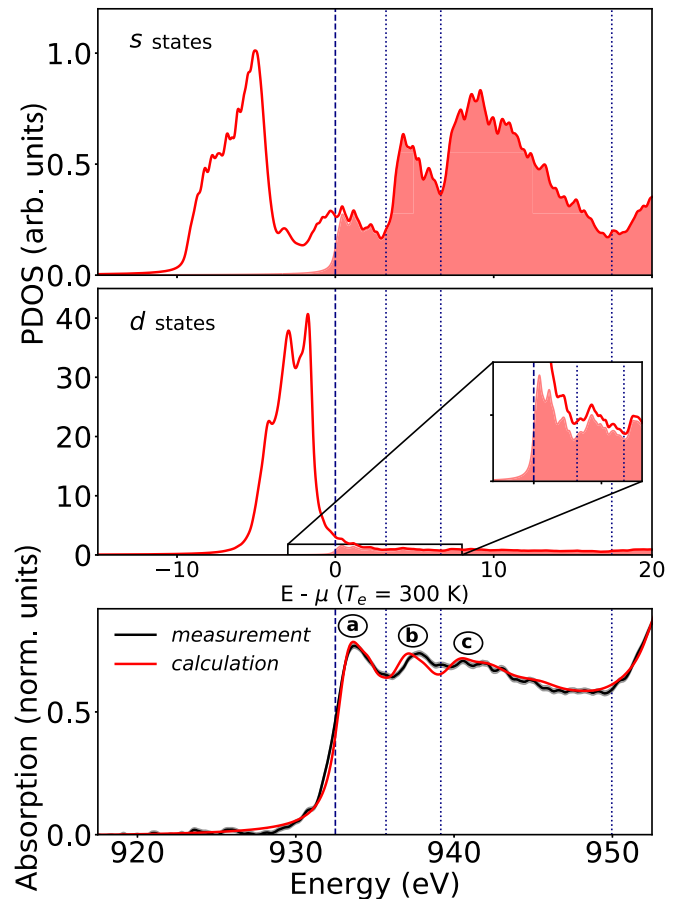


FIG. 2. (Upper panel) Projected density of state (PDOS) for copper at normal solid density  $\rho_0$  and at  $T_e = T_i = 300$  K for  $s$  and  $d$  channels. The colored areas correspond to the vacant electronic states. The  $d$  channel is zoomed because of the high amplitude of the  $3d$  band localized  $\sim 1.5$  eV below  $\mu(T_e = 300$  K). (Lower panel) Calculation of the XANES spectrum at  $L_3$  absorption edges of copper (red curve) compared to experiment in the same conditions (black curve).

The colored areas in Fig. 2 refer to the unoccupied DOS which is representative of the possible final states of the photoelectron transition. On this shaded part, we recognize the features in the electron DOS that are responsible for the three peaks (a), (b), and (c) localized between 930 eV and 940 eV in the XANES spectrum, as well as the minimum amplitude at  $\sim 20$  eV above  $\mu(T_e = 300$  K).

## II. SHAPE MODIFICATIONS INDUCED BY TEMPERATURE

To identify the shape modifications induced by the rise of the temperature, we carry out calculations of the x-ray absorption spectrum for several electronic and ionic temperatures at solid density. However, hydrodynamic expansion of thin targets can become significant after only a few picoseconds in ultrafast pump-probe experiments. To take this into account, we carry out simulations for density below the solid density to see if this density change has some influence on the modification induced by temperature.

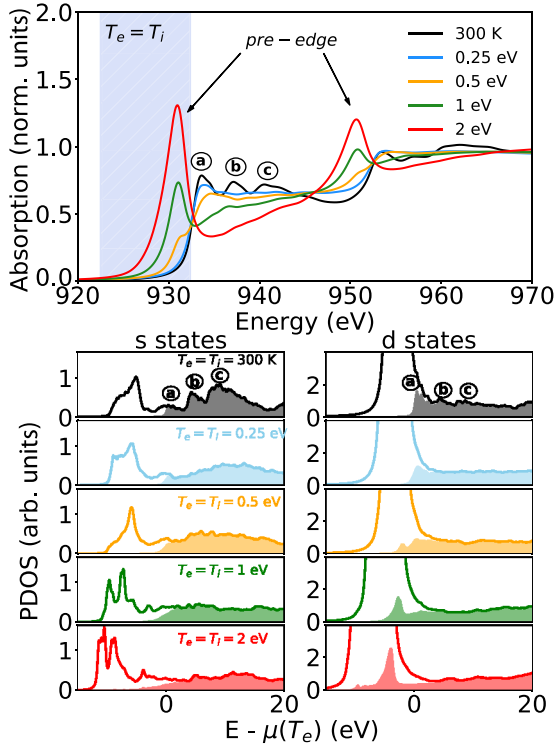


FIG. 3. (Upper panel) *Ab initio* XANES spectra at  $L_{2,3}$  absorption edges of copper at normal solid density  $\rho_0 = 8.9 \text{ g/cm}^3$  and at thermal equilibrium  $T_e = T_i$  up to  $T_e = 2 \text{ eV}$ . (Lower panel) Corresponding projected density of state (PDOS) on  $s$  and  $d$  channels. The colored areas correspond to the vacant electronic states.

#### A. Temperature dependence: At thermal equilibrium $T_e = T_i$

We start by simulations at thermal equilibrium where  $T_e = T_i$  at solid density  $\rho_0 = 8.9 \text{ g/cm}^3$ . Computed XANES spectra for temperatures up to  $2 \text{ eV}$  are reported in the upper panel of Fig. 3. For the temperature of  $0.25 \text{ eV}$ , the copper is melted (the melting being expected at  $0.117 \text{ eV} = 1358 \text{ K}$  at ambient pressure).

As the temperature increases, a pre-edge peak appears and is partially balanced by a reduction of the absorption just behind the edge. This behavior was also observed in Ref. [14] for temperature up to  $2 \text{ eV}$ . The intensity of this pre-edge structure is connected to the value of the electron temperature  $T_e$ . When increasing  $T_e$ , some electrons from the  $3d$  band, fully occupied in ambient conditions, are promoted towards higher energy states and above  $\mu(T_e)$ . Thus, the vacant states created below  $\mu(T_e)$  become available for photoionization.  $2p \rightarrow 3d$  transitions are then possible, and this induces the formation of a pre-edge structure in the XANES spectrum. It was observed that for transition metals, the  $L_{2,3}$  white line intensity can be explained on the basis of  $d$  vacancies [26]. This is also true for copper. The size of the pre-edge is connected to the shape of the electronic occupation, governed by Fermi-Dirac distribution  $f(\epsilon, \mu(T_e), T_e)$  defined as

$$f(\epsilon, \mu(T_e), T_e) = \frac{1}{1 + \exp\left(\frac{\epsilon - \mu(T_e)}{k_b T_e}\right)}. \quad (5)$$

It depends on both the energy  $\epsilon$ , the chemical potential  $\mu(T_e)$ , and the temperature  $T_e$ . The  $3d$  band is highly localized at ambient condition and keeps this property even at high temperatures as can be seen in the lower panel of Fig. 3. Copper has an fcc crystalline structure at normal conditions, and the local environment does not change strongly upon melting. The empty part of the  $3d$  band consequently appears as a thin peak also beyond melting temperature.

The absorption spectrum becomes, however, different above the edge. A loss of spectral structures in this region is clearly observed in Fig. 3 for  $T_e = T_i \geq 0.25 \text{ eV}$ , in close correlation with the loss of DOS structures above  $\mu(T_e)$  in the liquid state. As soon as the system turns to liquid, the structures labeled (b) and (c) on the XANES spectra and the PDOS vanish. The first peak (a) stays visible up to  $0.5 \text{ eV}$  and then disappears as the absorption is reduced in this region. The structures (b) and (c) might then be used to detect the loss of crystalline structure in copper but this would require further analysis to consolidate this observation. Note that these (b) and (c) structures are not comparable to EXAFS oscillation observable around  $30 \text{ eV}$  above the edge which are connected to the diffusion of photoelectrons on the neighbor atoms.

#### B. Electronic temperature dependence at $T_e \neq T_i = 300 \text{ K}$

To enhance the effect of  $T_e$  on the spectra without any influence from the atomic structure, we now focus on the electronic temperature dependence of the XANES spectra by performing simulations at different  $T_e$  up to  $2 \text{ eV}$  while keeping  $T_i$  at  $300 \text{ K}$  at the solid density  $\rho_0$ . The ionic structure is the fcc one obtained for the ions at  $300 \text{ K}$ . The computed spectra are presented in the upper panel of Fig. 4. As for the case  $T_e = T_i$ , the broadening of Fermi-Dirac distribution with  $T_e$  always leads to the depopulation of electronic states at the top of the  $3d$  band.

The structure referred to as (a) on these absorption spectra is strongly reduced as the electronic temperature  $T_e$  increases. The structures labeled (b) and (c) stay clearly visible up to the highest temperature simulated here.

The lower panel of Fig. 4 shows the corresponding  $s$  and  $d$  components of the PDOS. When increasing the electronic temperature  $T_e$  while keeping the same crystalline atomic structure, the general shape of the  $3d$  band is nearly unchanged. This is also true for the  $s$  component. The structures in the projected DOS connected to the peaks (b) and (c) of the XANES spectra are visible for all temperatures  $T_e$ . This confirms that the (b) and (c) structures are directly linked to the ionic structure, and that the pre-edge and structure (a) are representative of the electronic temperature  $T_e$ .

The DOS shape is different between thermally equilibrated and strong out-of-equilibrium cases (presented latter in Fig. 7). When copper turns from out-of-equilibrium fcc (ions at  $300 \text{ K}$ ) to liquid at thermal equilibrium ( $T_e = T_i$ ), the  $3d$  band stays localized but its shape is modified. That leads to slightly higher amplitude and thinner pre-edge structures for a given  $T_e$  when  $T_i = 300 \text{ K}$ . This can be seen by comparing the corresponding XANES spectra shown in Figs. 3 and 4. In all cases, areas stay comparable.

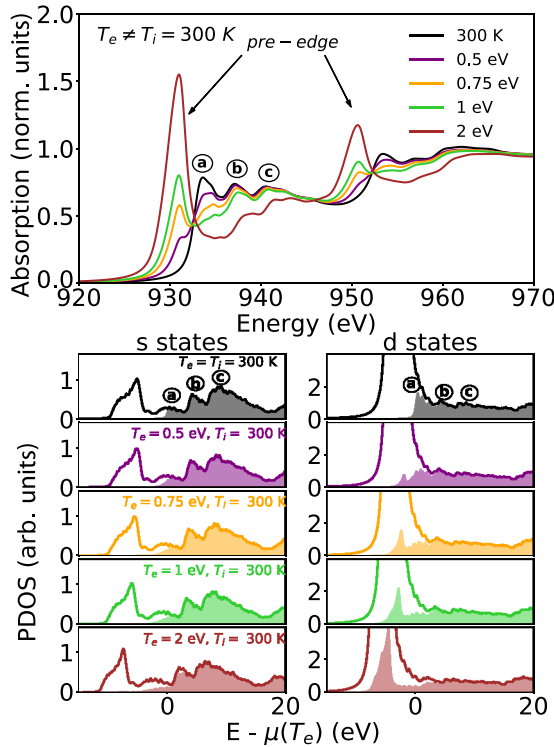


FIG. 4. (Upper panel) *Ab initio* XANES spectra at  $L_{2,3}$  absorption edges of copper at solid density  $\rho_0 = 8.9 \text{ g/cm}^3$  for strong out-of-equilibrium conditions  $T_e \gg T_i = 300 \text{ K}$  up to  $T_e = 2 \text{ eV}$ . (Lower panel) Corresponding projected density of state (PDOS) on  $s$  and  $d$  channels. The colored areas correspond to the vacant electronic states.

### C. Temperature dependence for expanded cases $\rho < \rho_0$

The question is now to evaluate the effect of the density on the signature of temperature in XANES spectra. Simulations for three different density values were therefore performed: at solid density  $\rho_0 = 8.9 \text{ g/cm}^3$ , liquid density  $\rho_{\text{liquid}} = 8 \text{ g/cm}^3$ , and at an expanded density of  $6 \text{ g/cm}^3$ .

Figure 5 shows the computed XANES spectra for the expanded case at  $\rho = 6 \text{ g/cm}^3$  and for equilibrated temperatures  $T_e = T_i$  up to  $2 \text{ eV}$ . We also observe the rise of the pre-edge

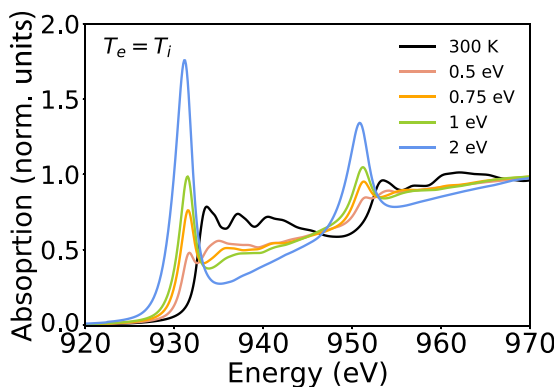


FIG. 5. XANES spectra at ambient conditions and for different temperatures in equilibrated situations ( $T_e = T_i$ ) for the expanded density  $\rho = 6 \text{ g/cm}^3$ .

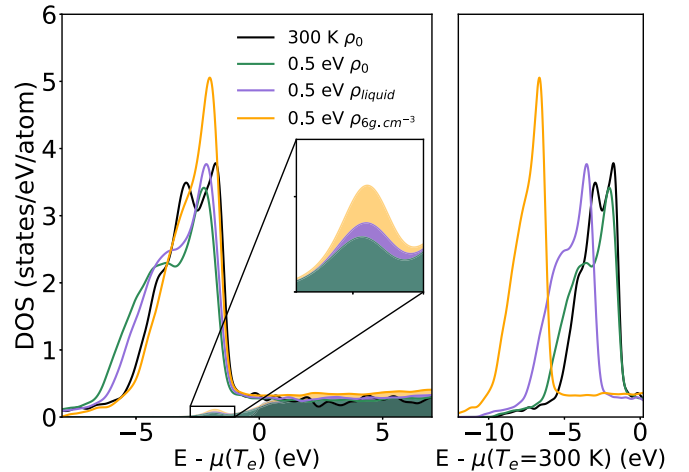


FIG. 6. (Left panel) Density of state (DOS) of copper at different densities for  $T_e = T_i = 0.5 \text{ eV}$  and compared to the one at ambient conditions. They are represented as a function of  $\epsilon - \mu(T_e)$ . The colored areas correspond to the vacant electronic states. The inset shows a zoom of the region inside the square around  $-2.5 \text{ eV}$ . (Right panel) Same DOS represented as a function of constant  $\epsilon - \mu$  ( $T_e = 300 \text{ K}$ )

structure with the electronic temperature  $T_e$ . Its amplitude value for a given temperature is slightly higher compared to XANES calculations at the solid density  $\rho_0$  reported in Figs. 3 and 4. The pre-edge is also thinner and the absorption level is lower above the absorption edge.

To interpret these observations, one can refer to the Fig. 6 showing the DOS for several densities as a function of  $\epsilon - \mu(T_e)$ . It appears that the  $3d$  band is not strongly modified, with both temperature and density. Therefore, the Fermi-Dirac distribution has similar impact on the  $3d$ -band occupation. This is clearly visible in the shaded areas showing the unoccupied DOS. The pre-edge structure keeps a similar shape in the absorption spectra at these lower densities (e.g., at  $\rho = 6 \text{ g/cm}^3$  in Fig. 5).

Looking more closely at Fig. 6, the  $3d$  band gets thinner at lower density and leads to a higher amplitude of the right side of this electronic band. Consequently, for a given temperature, the pre-edge amplitude becomes higher when the density decreases.

## III. XANES SPECTRA SHIFTS

The positions of the pre-edge and other peaks above the edge in the absorption spectrum are connected to the energy difference between the DOS and the  $2p$  orbital. Both undergo variations with temperature and density that we have to take into account to describe a possible energy shift of the absorption features when modifying the thermodynamical conditions. This is mandatory to be able to compare theoretical and experimental spectra.

### A. DOS and chemical potential shifts with temperature and density

A negative shift of the DOS is observed when the density is fixed and the temperature is increased. This effect is shown

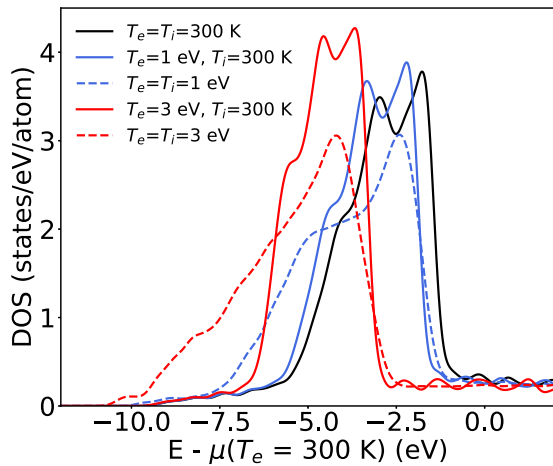


FIG. 7. Density of state (DOS) of copper at solid density  $\rho_0$  for both thermally equilibrated ( $T_e = T_i$ ) and strong out-of-equilibrium ( $T_e \gg T_i = 300$  K) conditions up to 3 eV.

in Fig. 7 for the solid density  $\rho_0$  and different temperatures, in both thermally equilibrated ( $T_e = T_i$ ) and strong out-of-equilibrium ( $T_e \gg T_i = 300$  K) situations. For a given electronic temperature, the energy shift is identical for these two situations.

The energy shift of the chemical potential  $\mu(T_e)$  is directly correlated to the DOS one, since  $\mu(T_e)$  is obtained by the conservation of the total number of electrons  $N_e = \int g(\varepsilon, T) f(\varepsilon, \mu(T_e), T) d\varepsilon$  with  $g(\varepsilon, T)$  the electronic DOS and  $f(\varepsilon, \mu(T_e), T)$  the Fermi-Dirac distribution. As can be observed in Fig. 8, the chemical potential increases with temperature and exceeds from around 2 eV its ambient value at  $T_e = 3$  eV and this is true for both cases  $T_e = T_i$  and  $T_e \gg T_i = 300$  K. Given the similar motions between these two cases, we might reasonably assume that the number of electrons in these localized  $3d$  bands is not different for a given temperature. The broadening of the Fermi-Dirac distribution and the negative DOS shift lead to an increase of the chemical potential. This was observed for transition metals with localized  $d$  states [27,28]. This is the opposite of the motion of the chemical potential computed for aluminum

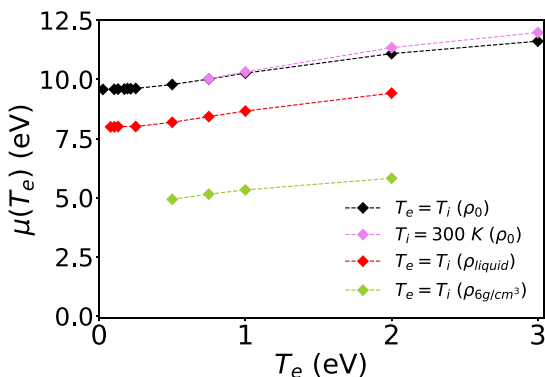


FIG. 8. Evolution of the chemical potential  $\mu(T_e)$  with the temperature of the electrons  $T_e$  for three densities of copper  $\rho = \rho_0$ ,  $\rho = \rho_{\text{liquid}} = 8$  g/cm<sup>3</sup>, and  $\rho = 6$  g/cm<sup>3</sup>.

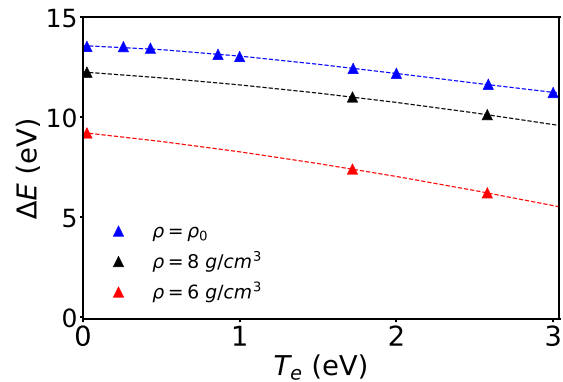


FIG. 9. Evolution of the energy difference  $\Delta E$  between  $2p$  orbital energies when considered in the frozen core or not.  $\Delta E$  is defined as  $E(2p_{\text{relaxed}}) - E(2p_{\text{atomic}})$  where  $E(2p_{\text{atomic}})$  corresponds to the value when the  $2p$  orbital is frozen.

and this could be traced back to the free-electron-like behavior of aluminum [2].

When the density is lowered, the density of state is also shifted towards lower energies for a given temperature as can be seen in the right panel of Fig. 6.

In parallel, the chemical potential drops due to the conservation of the total number of electrons  $N_e$  (see Fig. 8). In the expanded case, the  $3d$  states are even more localized than for the case at normal density. This was already observed for aluminum, where delocalized states becomes more atomiclike when density decreases. As a consequence, the chemical potential has to decrease to recover the right number of electrons for a given temperature [9]. This is a density effect. For a given density, even for the lowest density explored here, the chemical potential still increases with temperature.

## B. $2p$ orbital relaxation

When changes in temperature and/or density occur, the  $2p$  orbitals relax to different energies. This can result in possible XANES spectra shifts if the probed valence electronic states do not shift accordingly. This was observed for expanded aluminum and molybdenum [5,9].

We recall that all XANES calculations involve the frozen core approximation. The generation of the PAW data set using ATOMPAW and the energy value of the core orbitals result from an atomic calculation. To take into account the relaxation we generate a different PAW data set where only  $1s$  states are frozen. Relative variations  $\Delta E$  of relaxed  $2p$  orbital energies compared to the atomic value are shown in Fig. 9. We see here that  $\Delta E$  decreases when  $T_e$  rises for each density considered, meaning that  $2p$  orbital gets closer to the nucleus. This can be understood by the reduction of the electronic screening which leads to a more attractive electron-ion potential.

In these conditions, the highest shift of the  $2p$  orbital is  $-2.3$  eV for a temperature of 3 eV. This is almost the same value as the DOS shift illustrated on Fig. 7, and this holds for all the temperatures shown here. This is why we do not observe a visible shift on the XANES spectra presented before in Figs. 3 and 4.

Regarding the density effect,  $2p$  orbital energy also decreases when the density is lowered. Both the DOS (shown in Fig. 6) and the  $2p$  orbital move and almost in the same proportion (the maximum difference is 0.2 eV between the DOS and the  $2p$  shifts at  $\rho = 6 \text{ g/cm}^3$ ), which results in an unchanged position of the XANES spectra.

#### IV. EXTRACTING $T_e$ FROM X-RAY ABSORPTION SPECTRA

In warm dense Be [12] and Al [13], previous studies have demonstrated that the temperature induced  $K$  edge broadening could be fitted with a Fermi-Dirac distribution function to retrieve the value of the electronic temperature  $T_e$ . This methodology applies for a relatively flat energy profile of the electron DOS. It cannot be used for copper whose DOS is dominated by the strongly localized  $3d$  band.

We have evidenced that both density and temperature have influence on the electronic occupations dictated by  $f(\epsilon, \mu(T_e))$ . At the end, the variations in  $\mu(T_e)$  and the resulting changes in  $f(\epsilon, \mu(T_e))$  always lead to the depopulation of electrons of the  $3d$  band, giving a pre-edge structure in the XANES spectra. The same phenomenon is observed for all the calculations we have performed, i.e., both  $(T_e, T_i)$  temperatures up to 3 eV, and densities ranging from solid density  $\rho_0$  to densities as low as  $\rho = 6 \text{ g/cm}^3$ . The question is then can we use this pre-edge to deduce the value of the electronic temperature?

For this purpose, we consider the value of the spectral integral of the pre-edge. This integral is proportional to the number of unoccupied electronic states in the DOS. Figure 3 shows through the hatched area the energy region considered for such pre-edge integration (from 922.5 eV to 932.5 eV). The choice for integration region is arbitrary. The value of the integral of the cold spectrum in this spectral region is subtracted to the integral in each case. The integral is not equal to zero in the cold case even if no electron is thermally excited because of the spectral linewidth and the experimental broadening of the absorption edge. Spectral resolution and natural linewidth could modify the height; this is why we choose to use the integral instead. Note that we compute the evolution of the pre-edge area referred to as the cold case. This, also, removed potential experimental resolution and natural linewidth effect assuming that they are the same for the different conditions explored here. Looking at the comparison between experimental and theoretical spectra for cold and hot conditions presented in Fig. 4(b) in our previous paper [15], one can see that the agreement is really good for both temperatures showing that these approximations seem reasonable.

Using our *ab initio* XANES calculations performed for several temperatures at thermal equilibrium  $T_e = T_i$ , out-of-equilibrium  $T_e \neq T_i$ , and for three different copper densities, we have computed the value of the pre-edge integral for each spectrum and so for each electronic temperature  $T_e$ . The results are presented in Fig. 10. Below  $T_e = 0.2 \text{ eV}$ , the pre-edge is too weak to be quantified and its evolution is not monotonous. Above 0.2 eV, the evolution of the pre-edge integral with  $T_e$  is monotonous. More remarkable, it does not depend significantly on the equilibrium versus nonequilibrium condition, and depends little on the density. The amplitude

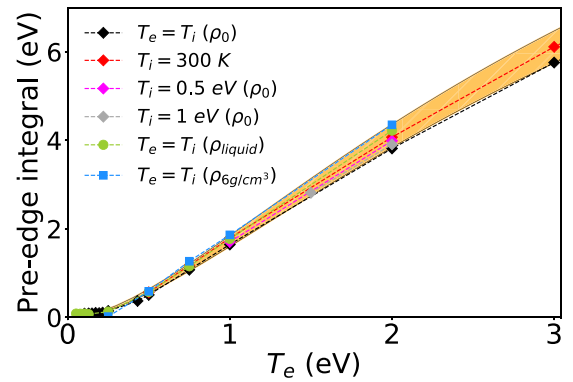


FIG. 10. Evolution of the pre-edge integral as a function of the electronic temperature  $T_e$  for all the simulated conditions.

of the pre-edge changes but not the area of the pre-edge. At the end, the difference in the integral value reaches  $\sim 15\%$  at  $6 \text{ g/cm}^3$  compared to  $8.9 \text{ g/cm}^3$ .

Above  $T_e = 0.2 \text{ eV}$ , as the evolution of the pre-edge integral is monotonous, it is possible to establish an unambiguous relationship between  $T_e$  and the pre-edge integral. This relationship has been recently used to measure the electron temperature dynamics of laser-heated copper with a picosecond time resolution [15]. To be able to recover directly electronic temperature from experimental spectra, the requirement is to use for the integration exactly the same region as was chosen for theoretical spectra.

#### V. CONCLUSION

In summary, we calculated x-ray absorption spectra near  $L_{2,3}$  edges of warm dense copper based on first-principle electronic structure calculations and molecular dynamics simulations. By introducing a variable width to model the linewidth, we obtain a good description of the experimental XANES spectrum and its modulations at room temperature.

We explain the modifications induced by both electron and ion temperatures and density on XANES spectra at the microscopic level. The shape is modified in two ways. First, as copper is a noble metal with almost filled  $3d$  states at ambient conditions, they do not appear on XANES spectrum near the  $L$  edge at ambient condition. But, when the temperature of the electrons  $T_e$  increases, the  $3d$  states are partially depopulated, leading to a pre-edge on the absorption spectrum and a reduction of the absorption behind the edge. The amplitude and shape of the pre-edge is directly linked to the modification of  $3d$  electronic population. Second, the modulations above the edge disappear when the temperature increases as solid copper turns to a liquid state. This opens a promising perspective to the experimental study of phase transition dynamics in nonequilibrium warm dense transition metals. This observation would require further investigation. In the range of investigation (temperature up to 3 eV and density as low as  $6 \text{ g/cm}^3$ ), we do not observe any energy shift of the XANES spectra, as the  $2p$  core level shift is balanced by the DOS one.

The spectral integral of the pre-edge can be used to deduce the electronic temperature  $T_e$  for a wide range of temperatures

and densities. This leads to a useful tool to associate an electronic temperature  $T_e$  to experimental XANES spectra. This tool can be used for any measurement of XANES spectra for femtosecond laser-heated copper without the need of additional calculations keeping in mind that the same integral region has to be chosen to analyze the experimental spectra. The same considerations can be applied regarding the  $d$  band of the other noble metals (Ag and Au). It could be possible to extract the electronic temperature in a similar way for other transition metals with localized  $d$  states.

We believe that for any material, there should be a direct connection between the electronic temperature and the shape on the XANES spectra. Then, there is always a way

to directly *read* the temperature on XANES spectra. The signature will depend on the DOS. As soon as there are no localized states near the Fermi level, the temperature could be extracted directly by fitting a Fermi-Dirac function to the edge. If there are localized states near the Fermi level as for the transition metals, the temperature will appear as a pre-edge or a shoulder. For all cases, one needs first dedicated simulations to quantify the change induced by temperature.

#### ACKNOWLEDGMENT

The authors are extremely grateful to M. Torrent for his precious help for the implementation in the ABINIT code.

- 
- [1] F. Dorchie and V. Recoules, *Phys. Rep.* **657**, 1 (2016).
- [2] V. Recoules and S. Mazevet, *Phys. Rev. B* **80**, 064110 (2009).
- [3] B. I. Cho, K. Engelhorn, A. A. Correa, T. Ogitsu, C. P. Weber, H. J. Lee, J. Feng, P. A. Ni, Y. Ping, A. J. Nelson, D. Prendergast, R. W. Lee, R. W. Falcone, and P. A. Heimann, *Phys. Rev. Lett.* **106**, 167601 (2011).
- [4] F. Dorchie, A. Lévy, C. Goyon, P. Combis, D. Descamps, C. Fourment, M. Harmand, S. Hulin, P. M. Leguay, S. Petit, O. Peyrusse, and J. J. Santos, *Phys. Rev. Lett.* **107**, 245006 (2011).
- [5] F. Dorchie, V. Recoules, J. Bouchet, C. Fourment, P. M. Leguay, B. I. Cho, K. Engelhorn, M. Nakatsutsumi, C. Ozkan, T. Tschentscher, M. Harmand, S. Toleikis, M. Störmer, E. Galtier, H. Lee, B. Nagler, P. Heimann, and J. Gaudin, *Phys. Rev. B* **92**, 144201 (2015).
- [6] A. Mancic, A. Lévy, M. Harmand, M. Nakatsutsumi, P. Antici, P. Audebert, P. Combis, S. Fourmaux, S. Mazevet, O. Peyrusse, V. Recoules, P. Renaudin, J. Robiche, F. Dorchie, and J. Fuchs, *Phys. Rev. Lett.* **104**, 035002 (2010).
- [7] P. M. Leguay, A. Lévy, B. Chimier, F. Deneuville, D. Descamps, C. Fourment, C. Goyon, S. Hulin, S. Petit, O. Peyrusse, J. J. Santos, P. Combis, B. Holst, V. Recoules, P. Renaudin, L. Videau, and F. Dorchie, *Phys. Rev. Lett.* **111**, 245004 (2013).
- [8] A. Benuzzi-Mounaix, F. Dorchie, V. Recoules, F. Festa, O. Peyrusse, A. Lévy, A. Rivasio, T. Hall, M. Koenig, N. Amadou, E. Brambrink, and S. Mazevet, *Phys. Rev. Lett.* **107**, 165006 (2011).
- [9] A. Lévy, F. Dorchie, A. Benuzzi-Mounaix, A. Rivasio, F. Festa, V. Recoules, O. Peyrusse, N. Amadou, E. Brambrink, T. Hall, M. Koenig, and S. Mazevet, *Phys. Rev. Lett.* **108**, 055002 (2012).
- [10] C. Marini, F. Occelli, O. Mathon, R. Torchio, V. Recoules, S. Pascarelli, and P. Loubeyre, *J. Appl. Phys.* **115**, 093513 (2014).
- [11] M. Harmand, A. Rivasio, S. Mazevet, J. Bouchet, A. Denoed, F. Dorchie, Y. Feng, C. Fourment, J. G. E. Galtier, F. Guyot, R. Kodama, M. Koenig, H. J. Lee, K. Miyanishi, G. Morard, R. Musella, B. Nagler, M. Nakatsutsumi, N. Ozaki, V. Recoules, S. Toleikis, T. Vinci, U. Zastra, D. Zhu, and A. Benuzzi-Mounaix, *Phys. Rev. B* **92**, 024108 (2015).
- [12] W. Schwanda and K. Eidmann, *Phys. Rev. Lett.* **69**, 3507 (1992).
- [13] F. Dorchie, F. Festa, V. Recoules, O. Peyrusse, A. Benuzzi-Mounaix, E. Brambrink, A. Levy, A. Rivasio, M. Koenig, T. Hall, and S. Mazevet, *Phys. Rev. B* **92**, 085117 (2015).
- [14] B. Cho, T. Ogitsu, K. Engelhorn, A. Correa, Y. Ping, J. W. Lee, L. J. Bae, D. Prendergast, R. Falcone, and P. Heimann, *Sci. Rep.* **6**, 18843 (2015).
- [15] N. Jourdain, L. Lecherbourg, V. Recoules, P. Renaudin, and F. Dorchie, *Phys. Rev. B* **97**, 075148 (2018).
- [16] The ABINIT code is a common project of the Université Catholique de Louvain, Corning Inc., Commissariat à l’Energie Atomique, Université de Liège, Mitsubishi Chemical Corp., and other contributions [<http://www.abinit.org>].
- [17] X. Gonze, B. Amadon, P. Anglade, J. Beuken, F. Bottin, P. Boulanger, F. Bruneval, D. Caliste, R. Caracas, M. Côté, T. Deutsch, L. Genovese, P. Ghosez, M. Giantomassi, S. Goedecker, D. Hamann, P. Hermet, F. Jollet, G. Jomard, S. Leroux, M. Mancini, S. Mazevet, M. Oliveira, G. Onida, Y. Pouillon, T. Rangel, G. Rignanese, D. Sangalli, R. Shaltaf, M. Torrent, M. Verstraete, G. Zerah, and J. Zwanziger, *Comput. Phys. Commun.* **180**, 2582 (2009).
- [18] F. Bottin, S. Leroux, A. Knyazev, and G. Zerah, *Comput. Mater. Sci.* **42**, 329 (2008).
- [19] J. P. Perdew and Y. Wang, *Phys. Rev. B* **45**, 13244 (1992).
- [20] A. Dewaele, M. Torrent, P. Loubeyre, and M. Mezouar, *Phys. Rev. B* **78**, 104102 (2008).
- [21] M. Taillefumier, D. Cabaret, A.-M. Flank, and F. Mauri, *Phys. Rev. B* **66**, 195107 (2002).
- [22] O. Bunau and M. Calandra, *Phys. Rev. B* **87**, 205105 (2013).
- [23] N. Holzwarth, A. Tackett, and G. Matthews, *Comput. Phys. Commun.* **135**, 329 (2001).
- [24] V. Mauchamp, M. Jaouen, and P. Schattschneider, *Phys. Rev. B* **79**, 235106 (2009).
- [25] M. O. Krause and J. H. Oliver, *J. Chem. Ref. Data* **8**, 329 (1979).
- [26] T. Miyamoto, H. Niinmi, Y. Kitajima, and K. Asakura, *Coordination Chemistry Review* **272-278**, 44 (2014).
- [27] B. Holst, V. Recoules, S. Mazevet, M. Torrent, A. Ng, Z. Chen, S. E. Kirkwood, V. Sametoglu, M. Reid, and Y. Y. Tsui, *Phys. Rev. B* **90**, 035121 (2014).
- [28] E. Bevilion, J. P. Colombier, V. Recoules, and R. Stoian, *Phys. Rev. B* **89**, 115117 (2014).